Journal of Magnetic Resonance **151,** 48–59 (2001)
doi:10.1006/jmre.2001.2353, available online at http://www.idealibrary.com on IDEAL®

A General Strategy for the NMR Observation of Half-Integer Quadrupolar Nuclei in Dilute Environments

Andrew S. Lipton, Jesse A. Sears, and Paul D. Ellis[1]

Macromolecular Structure and Dynamics Directorate, WR Wiley Environmental Molecular Sciences Laboratory, Pacific Northwest National Laboratory, Richland, Washington 99352

E-mail: paul.ellis@pnl.gov

Received October 16, 2000; revised March 2, 2001

A general strategy for the observation of low γ half-integer quadrupolar nuclides in biological systems is presented. The methodology combines low-temperature (4–100 K) techniques with cross-polarization (CP) experiments while employing a so-called Carr–Purcell–Meiboom–Gill spin-echo sequence (CPMG). This combined approach is termed CP/QCPMG. Also discussed are data processing issues that are unique to the induced signals that result from the QCPMG pulse sequence. Central to this strategy is the development of a stable low-temperature (4 to 250 K) NMR double-resonance probe. The probe is robust enough to handle multiple contact experiments and long acquisition periods with ^{1}H decoupling. This approach is illustrated with low-temperature solid-state ^{67}Zn and ^{25}Mg NMR CP/QCPMG experiments on model compounds. The conclusion reached is that the strategy affords sufficient sensitivity to examine Zn^{2+} and/or Mg^{2+} binding sites in metalloproteins.

INTRODUCTION

The main focus of this paper is to describe and illustrate an overall strategy for the observation of half-integer quadrupolar nuclides ($^{67}Zn^{2+}$, $^{25}Mg^{2+}$, $^{63/65}Cu^{1+}$, etc) in dilute environments, specifically in metalloproteins. As a concrete example the discussion will be focused on zinc, which is found in relatively low abundance in nature, e.g., nominally 70 ppm in the Earth's crust and approximately 0.01 ppm in sea water (*1*). However, despite its low abundance, zinc plays an essential role in biology in the form of zinc metalloproteins and as a regulatory agent in homeostasis. In metalloproteins zinc can have a structural role, facilitated by its propensity to occupy tetrahedral (and less commonly octahedral or pentacoordinated) sites (*2*), or catalytic properties that take advantage of Zn^{2+} cation's intermediate value of hardness or softness. This intermediate hardness introduces an element of flexibility into the Lewis acidity of the Zn^{2+} cation. Several reviews on this aspect of zinc chemistry have been published (*1–3*).

Of particular interest here are the spectroscopic properties of zinc. Zinc belongs to a large class of elements (including Cu^{1+}, Cd^{2+}, Mg^{2+}, Ca^{2+}, and Be^{2+}) that in their common oxidation states are spectroscopically silent. In virtually all of it's chemistry, zinc is in the $+2$ oxidation state and as a result has a d^{10} electron configuration. With this electron configuration there are no *d–d* electronic excitations, making electronic spectroscopy of Zn^{2+} uninformative with regard to coordination environment. Further, since the electrons are all paired, EPR cannot be utilized to investigate Zn^{2+} ions in biological environments. Zinc does possess a magnetic moment (0.214 of that for ^{1}H) with a nuclear spin of $\frac{5}{2}$ and a modest NMR resonance frequency, 25.03 MHz in a field of 9.4 T (400 MHz for ^{1}H). The size of the magnetic moment implies low sensitivity; however liquid state ^{67}Zn NMR experiments can be and have been performed (*4*). The concentrations of the Zn^{2+} are typically high, >0.1 M, but lower concentrations can be utilized with isotropic enrichment. Also, due to the quadrupolar nature of the nuclide, the solution NMR lineshapes can become broad, making the NMR experiment more difficult with biological and nonbiological systems alike. With these nuclear properties, it is no wonder that the literature of ^{67}Zn NMR is sparse, and of those only a few are relevant to biology (*5*).

Historically, solid state ^{67}Zn NMR has been undesirable due to broad quadrupole lineshapes and low sensitivity (*6*). In recent years, however, dramatic improvements in the solid state NMR of quadrupolar nuclides have taken place. Notable among these improvements is the development of the means to significantly narrow the central transition of half-integer spin quadrupolar nuclides via methods such as dynamic angle spinning (DAS) (*7*), double rotation (DOR) (*8*), and the multiple-quantum magic angle spinning (MAS) experiments (*9*). To say that these experiments have had a profound impact in this field of spectroscopy (and their corresponding area of science to which they are applicable) would be an understatement. However, they suffer from one consistent draw back, namely sensitivity. In the case of DAS and the multiple-quantum MAS methodology, the line narrowing is accomplished in a "subtractive" fashion. That is, the

[1] To whom correspondence should be addressed.

1090-7807/01 $35.00

narrowed central transition is a few percent of the total integrated intensity of the central transition lineshape. In the case of DOR (setting aside its technical complications), the filling factor for the spins of interest is significantly poorer (perhaps by as much as a factor of 5) than that of standard NMR experiments, causing significant losses in sensitivity. For all three techniques, these sensitivity losses become significant only in those cases where the nucleus of interest is in a "rare" site or is diluted relative to normal compounds. It is this dilution effect that makes these techniques prohibitive for an insensitive nuclide such as ^{67}Zn, especially in a metalloprotein.

The consequences of dilution have a major impact as to whether a NMR experiment (using a fixed volume of sample) can be utilized in a biological system. As an example, consider a model compound for the active site carboxypeptidase A, zinc diimidazole diacetate, $Zn(Im)_2(OAc)_2$. The compound is 20.9% Zn by weight. Carboxypeptidase A is 0.19% Zn by weight. In going from the model compound to the protein a dilution of a factor of 110 has occurred. The spectroscopic challenge is to make up for this dilution factor!

The loss in sensitivity caused by dilution must be regained in such a way that the structural information is retained, i.e., the value of the quadrupole, shielding tensors, and their relative orientations. A large portion of this factor of 110 can be regained by going to low temperatures, i.e., $\sim$25 K. The effect of sample temperature on the observable signal will achieve a gain of about 12 in going from room temperature to 25 K due to the Boltzmann distribution. Additionally as the coil is also cooled to 25 K the resistance of the coil is lowered (*10*). The noise generated by the coil is proportional to the square root of both the wire resistance and temperature. Thus under ideal conditions the $S/N \propto (1/T)^{3/2}$, which includes the Boltzmann distribution and the noise figure of the coil. In practice S/N is limited by the noise figure of the receiver, in particular the noise contribution from the preamplifier. By utilizing a cryogenic preamplifier the dominant noise source has been shifted back to the probe, which can then potentially achieve the theoretical gain in S/N of a factor of $\sim$42 (*11*). The question then becomes, why not simply lower the temperature to 4.2 K and get the potential gain greater than 500? The answer is that the spin–lattice relaxation time, T_1, for the nucleus in question can become very long ($>$hours) at such low-temperatures. The longer T_1 becomes, the longer the wait between transients. Therefore, the real question is the S/N for a given time period. Hence, low-temperature is not the only answer. Low-temperature gains must be augmented by other signal enhancement methods, which can potentially reduce the consequences of T_1's, e.g., cross polarization (*12*). Further, these methods can be coupled with techniques that narrow the observed resonance while at the same time providing a means to recover the tensor information embedded within the overall lineshape.

Traditionally, MAS methods (*13*) have been utilized as means for increasing S/N by providing an averaging process, which transforms the static powder lineshape into a number of discrete sidebands. Basically, the integrated intensity of the powder lineshape is divided into a finite number of sidebands, providing a S/N gain while at the same time offering a means to recover tensor information (from the heights and/or areas of each of the sidebands). However, this method is technically difficult at low temperatures and the modest to high spinning speeds that are needed in the present context are not easy to obtain at the desired temperatures. Further, MAS methods also suffer the disadvantage that each spinning sideband is broadened significantly by the second-order quadrupole interaction. Another option is to employ a spin echo method, which accomplishes the same goal, namely a significant gain in sensitivity over powder methods while at the same time affording a recovery of the tensor information. The basic experiment is to Fourier transform (FT) the induced signal from a Carr–Purcell–Meiboom–Gill (CPMG) (*14*) echo train. Garroway (*15*) was the first to perform the experiment, which leads to an efficient separation of the inhomogeneous and homogeneous interactions. The Fourier-transformed data set consists of a manifold of sidebands. The lineshape of a given sideband is determined by the homogeneous interaction whereas the inhomogeneous interaction can be recovered by a detailed analysis of the sideband intensities. The proposed low-temperature experiments imply that the dynamic line-broadening processes will be absent. This results in narrow lines for the sidebands, yielding an even higher S/N, while providing the means to recover quadrupole, shielding tensors, and their relative orientation. The theory (*16*) of this experiment has been examined rigorously, with the aim of recovering the tensor information from the resulting lineshape and will not be discussed here.

Recently, we (5h) and our collaborators (5i) have applied this method to simple zinc compounds with the aim of illustrating the QCPMG method and its sensitivity with room temperature experiments. This paper will focus on the combination of this spin echo approach with CP while employing low-temperature techniques. Also presented here is the design of a low-temperature NMR probe that is double tuned for low-γ nuclides and ^{1}H at 9.4 T.

EXPERIMENTAL METHODS

Over the past couple of years, all of the experiments described here have been performed on three systems: a homebuilt/TecMag hybrid, a Varian Unity Plus, and a Varian Infinity Plus console while utilizing nonstandard power amplifiers and a homebuilt probe. The data reported here were obtained using the Infinity Plus console. The RF power amplifiers utilized consisted of an ENI LPI-10 (Electronic Navigation Industries, Inc., 3000 Winton Road South, Rochester, NY 14623) and Amplifier Systems CE400 (P.O. Box 280370, 18307 Napa Street, Northridge, CA 91325) for the low- and high-frequency, respectively, portions of the double-resonance experiment. Typical power conditions are 460 and 100 W for the low and high frequencies, respectively. Such powers, typically correspond to nonselective $\pi/2$ pulses of 6 and 4.2 μs, respectively, for ^{67}Zn (as well as

^{25}Mg) and ^{1}H, respectively. The low-temperature experiments utilized an Oxford CF-1200 cryostat in combination with an Oxford ITC-503 (Oxford Instruments, Eynsham Witney, Oxon, OX8 1Tl, England) temperature controller. Long-term temperature stability was on the order of ± 0.1 K; utilizing a 250-L dewar of $He_{(l)}$ the probe has operated stably for a period of up to a week.

PROBE DESCRIPTION

The Oxford Instruments CF-1200 cryostat has a continuous operating range of 3.8–500 K (lower temperatures can be achieved in "single-shot" mode). Ideally the probe had to meet the following criteria:

(1) unattended operation at cryogenic temperatures for extended periods of time;
(2) must fit into an Oxford CF-1200 cryostat, which has an inner diameter of 49 mm;
(3) must be vacuum tight; and
(4) must have a low heat load at liquid He temperatures.

A transmission line probe design was chosen for two principal reasons: to remove the tuning elements from the cryogenic environment, and to maximize the utilization of the limited space (49 mm diameter) provided by the Oxford cryostat. The cryostat itself was built to fit inside a standard widebore Oxford magnet (89 mm bore). The transmission lines (*17*) used in building the probes were constructed out of $\frac{1}{2}''$ stainless steel tubing (with an impedance of 72 Ω) for its low thermal conductivity and therefore lower heat load in the probe. Since the Oxford cryostat operates at negative pressure (1–10″ of Hg), the inner conductor of the transmission lines is sealed at the top. Tight-fitting PTFE plugs are used as spacers, four per transmission line. Based on stainless steel's calculated series resistance at 4 K, the Q of the probe will be significantly reduced as the temperature of the probe decreases. To better improve the performance of the probe, the inner conductors of the transmission lines were plated with silver (0.025 mm or ~2 skin depths). The minimum length of the transmission lines was determined by the length of the cryostat, and there is 1200 mm from the center of field to the top of the cryostat. Following McKay (*18*), the calculated transmission line length of 1308 mm was required to allow the use of standard capacitor values.

The schematic drawing of the probe circuit is depicted in Fig. 1. Due to the distance between the sample coil (L1) and the tuning elements (1308 mm), a higher coil inductance (6-turn, 100 nH) was required to reduce the effects of lead inductance introduced by the transmission lines. To improve filling factor and RF homogeneity, a 5-mm diameter coil was chosen with a length of 12 mm. C1 and C2 are the proton tune and match caps. The trap (series resonance), consisting of inductor L2 (2-turn, 5 mm diameter, 20 nH) and capacitor C3 (resonant at 400 MHz), serves two functions: to isolate the "X" and "H" sides, and to serve as the grounding point for the ^{1}H side. This

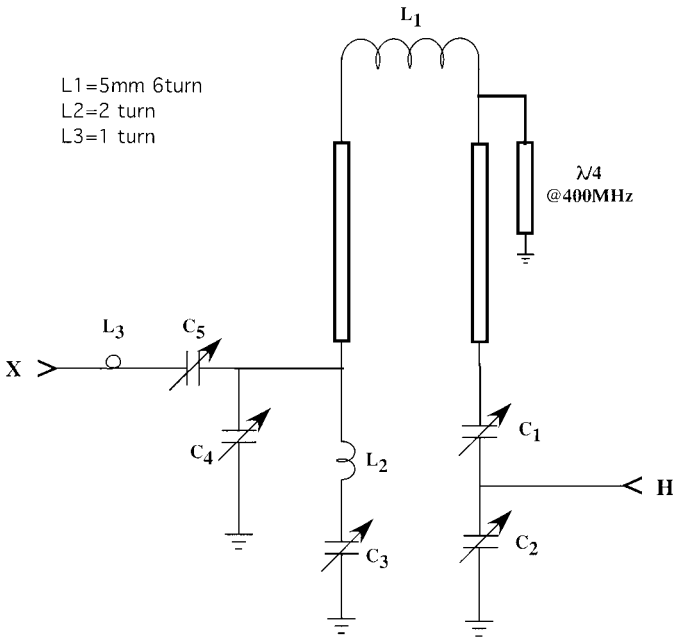

FIG. 1. Schematic drawing of the probe circuit.

trap also improves the overall Q of the probe. On the "X" side of the probe, C4 and C5 serve as the tune and match capacitors. The inductor L3 (1-turn, 5 mm diameter) is used to increase the isolation between "X" and "H"; a shorted $\lambda/4$ line serves as the X ground. Capacitors C1, C2, and C3 are Voltronics NMNT1012E PTFE trimmer caps, whereas C4 and C5 are Jennings gas variable capacitors CHV1N-45-0105. The tuning range of the low-frequency side is about 24 to 32 MHz, and as a consequence of the electrical length of the transmission lines we can also tune from 85–108 MHz. The ^{1}H tuning range is about 10 MHz and centered at 400 MHz.

Because the sample coil is at reduced temperatures (<200 K), the preamplifier is the dominant noise source in the system. By using a preamplifier with a low-noise temperature (77 K or lower) the signal-to-noise ratio of the system can be improved by as much as a factor of 2. The noise reduction is realized relative to spectra obtained with the standard system preamplifier (noise figure of 1.3 dB) by utilizing a cryogenic (77 K, liquid N_2) preamplifier supplied by Miteq (GaS FET, model AFS2, 25–30 MHz) that has a nominal noise figure of 0.2 dB.

RESULTS AND DISCUSSION

The performance of the probe from 20 to 200 K using the above design was as follows: ^{1}H/2 pulse width of 4.5 μs with 100 W, and a ^{67}Zn nonselective $\pi/2$ pulse width of 6 μs with 460 W. Cross-polarization was possible at that proton field strength due to the reduced power necessary for a Hartmann–Hahn match (*19*) of the quadrupolar zinc ($\gamma_{\mathrm{H}} B_{1\mathrm{H}} = \gamma_{\mathrm{X}} B_{1\mathrm{X}} * [I(I+1) - m(m-1)]^{1/2}$) (*20*). For the central transition ($m = \pm\frac{1}{2}$) of

^{67}Zn ($I = \frac{5}{2}$) the match condition is threefold less in RF field strength or $3\gamma_{Zn}B_{1Zn} = \gamma_H B_{1H}$, which corresponds to a factor of 9 reduction of power. There were no problems with Helium ionization when operating at low temperature as the sample area is under a partial vacuum and the tuning elements are at ambient conditions (air, temp, and pressure). However, the probe does require a modest flow (1–1.5 L/h of liquid helium) of cooling gas/liquid through the sample area for stable operation. For high-duty cycle experiments the probe will detune in the absence of such a flow rate, but with the proper flow at reduced temperature the probe tuning is stable.

Due to materials within the Oxford cryostat, the resonance frequency of a given nucleus has shifted roughly 20 ppm. This raw shift was measured at room temperature for both ^{67}Zn and ^{1}H by comparison of the isotropic chemical shifts between the current LT probe and cryostat and a commercial wideline probe (no shielding other than the aluminum can). This behavior was also determined to be temperature dependent and is illustrated in Fig. 2 with the Bloch decay ^{1}H resonances of solid zinc acetate dihydrate. Plotted are the ^{1}H frequencies (in kilohertz) relative to their values at 50 K *vs* absolute temperature over the range of 20 to 300 K. The outer curves are simply the fit to the observed doublet in the ^{1}H NMR of solid zinc acetate dihydrate. The middle curve is the fit to the average of the doublet frequencies, taken as the center of the lineshape, as a function of temperature. The fitted equation of the latter is

$$y = 11.278 - 0.309T + 0.001T^2. \quad [1]$$

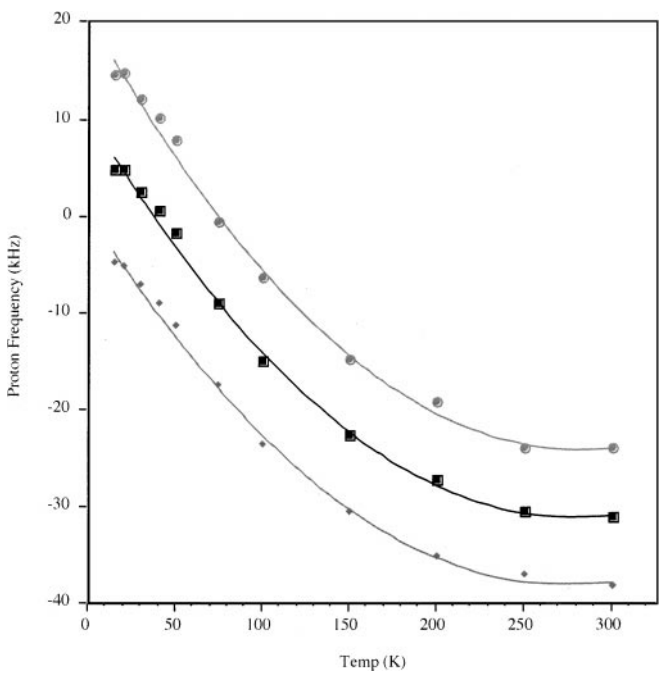

FIG. 2. Temperature dependence of the ^{1}H spectrum of solid zinc acetate dihydrate.

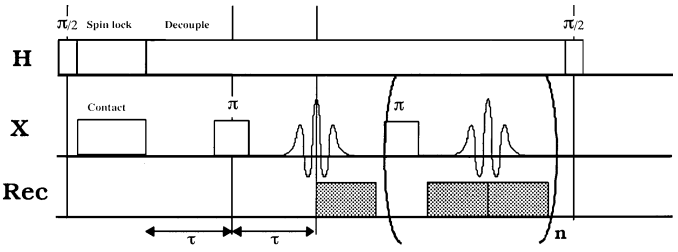

FIG. 3. CP/QCPMG pulse sequence.

This equation is useful for determination of the proper ^{1}H decoupling frequency in the temperature range given. Also note that the isotropic chemical shifts reported for any nuclide must be corrected using this or a similar function on a parts-per-million scale.

The timing diagram of the combined CP/QCPMG pulse sequence is depicted in Fig. 3. As shown, the induced signal in the receiver is not a free induction decay; rather it is constructed by the train of the 180° pulses. There are defined delays (typically 100–200 μs) around the pulses to remove the effects of RF blanking and the consequences of probe ringing. The following discussion demonstrates the advantages of using the combined CP and QCPMG (or spikelet) experiment with the ^{67}Zn NMR of an enriched sample of $Zn(OAc)_2 \cdot 2H_2O$ at 50 K. The signal enhancements achieved are demonstrated by the comparison of the integral and S/N of the Bloch decay echo (quadrupole echo, QE; recycle time, 30 s), QCPMG (recycle time, 30 s), CP/echo (recycle time, 5 s) and the CP/QCPMG (recycle time, 5 s) after 64 accumulations using the *same* receiver gain in each experiment. Figures 4a–4c (bottom to top) shows the results of the QE, QCPMG, and the CP/echo experiment. All of these data are plotted at the same vertical scale. Figure 4d contains the result of a CP/QCPMG experiment with the vertical scale *reduced* by a factor of 4. The processing conditions for the QE and the CP/echo experiment are the same (100 Hz of exponential line broadening) but different from the QCPMG and CP/QCPMG experiments (5 Hz of exponential line broadening). As expected the integrals are nearly identical between the QE and the QCPMG data; however there was a gain in S/N of ~3 in comparing the QCPMG echo to the conventional QE. Using CP to generate the initial magnetization gives a gain in S/N of ~12 over QE. The expected aggregate S/N for the combined CP/QCPMG experiment would be the product of the two previous gains or a factor ~36. Comparing Figs. 4a and 4d shows a gain ~46 for the combined experiment over the standard QE. The difference reflects the errors in comparing S/N ratios between spectra that are processed differently and the large difference between signal intensities. Another worthy notation is that the gain in sensitivity from using the QCPMG experiments is dependent upon the echo spacing. For example, in these data 500-Hz spacing was chosen, but with a spacing of 1 or 2 kHz one could gain even more sensitivity. The tradeoff is sacrificing information about

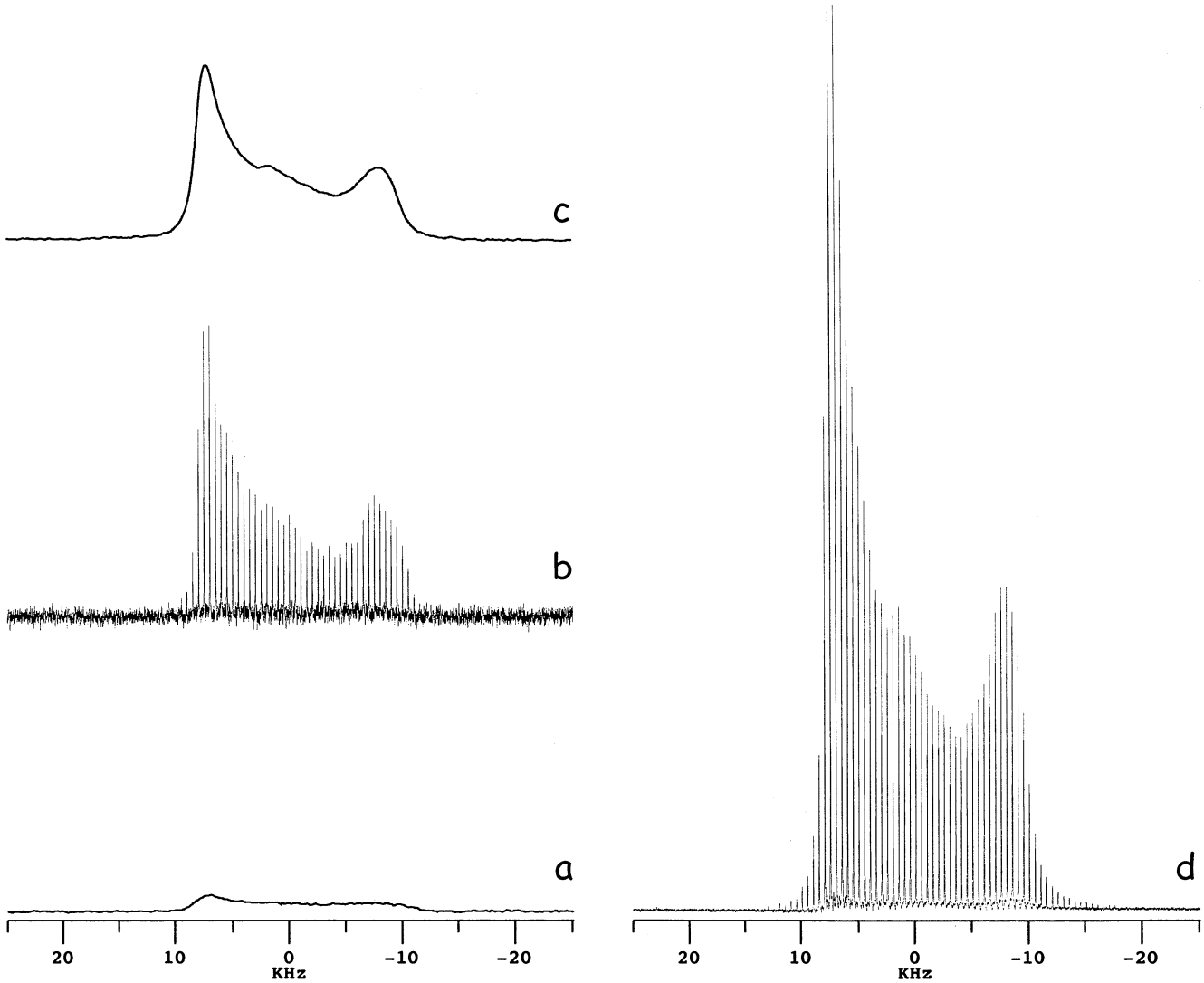

FIG. 4. ^{67}Zn experiments at 50 K on isotopically enriched (88%) $^{67}Zn(OAc)_2 \cdot 2H_2O$: (a) QE spectrum, (b) QCPMG spectrum, (c) CP/echo spectrum, and (d) CP/QCPMG spectrum reduced by a factor of 4.

the overall lineshape, which means there is a balance that must be achieved between sensitivity and the ability to recover accurate tensor information. The reader may also note the difference in the lineshape for zinc acetate dihydrate from previously published results (*6*); however this is due to a reversible phase transition (*21*). We have not made any interpretation of the resulting lineshape other than to note overall integrals (i.e., sensitivity) versus temperature.

Consider now the current level of isotopic enrichment commercially available for ^{67}Zn, which is 88%, versus the natural abundance of 4.11%. This represents a ~22-fold loss in the observable signal or a factor 484 in time to regain the same signal to noise. However, we have just shown that one can achieve a factor of 36–46 in recovery by utilizing the CP/QCPMG over the more traditional QE. Figure 5 contains the induced signal (256 transients, recycle time 5 s) from the CP/QCPMG sequence and its resulting Fourier transform on a natural abundance sample of zinc acetate dihydrate (112.7 mg) at 50 K. The total time needed to acquire the data was ~21 min. There are a couple of points associated with the induced signal that warrant attention. The signal represents the application of 100 spin echoes with a full echo period of 1 ms (for a 100-ms acquisition time). During this long acquisition time the decoupler was on at the same power levels utilized for CP, with no signs of probe degradation or arcing. Also, as the linewidth in the frequency domain is inversely proportional to the duration of the time domain response, there are 10-Hz spikelets separated by 1 kHz. This width is a reflection of the high crystallinity of the sample and the absence of any homogeneous interactions (and the long T_2 at this temperature).

We now intend to extend this combined methodology to the determination of both quadrupole and shielding tensors and their relative orientations in biological systems. Summarized

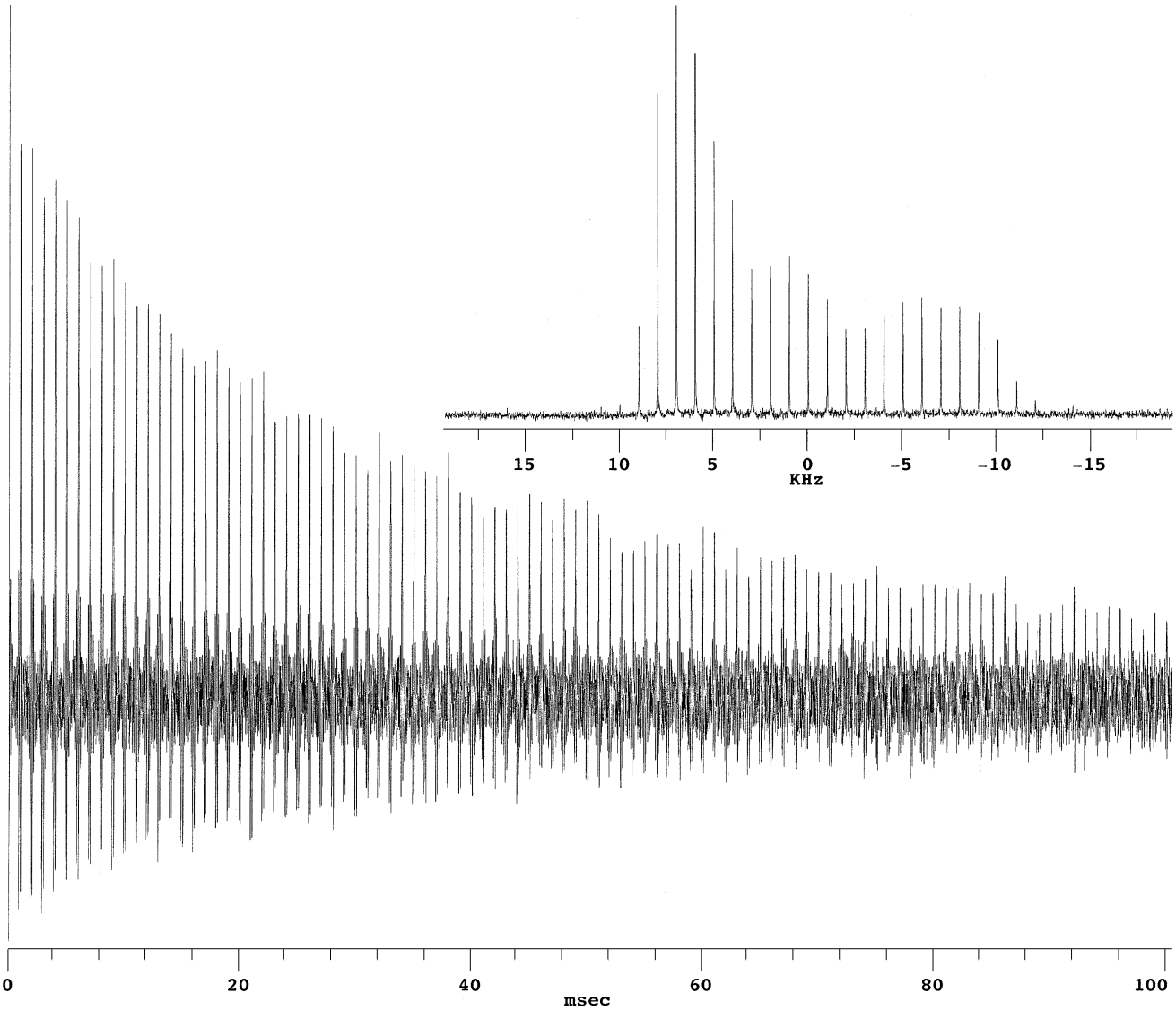

FIG. 5. The time domain signal is the result of 256 accumulations of a CP/QCPMG pulse sequence applied to 112.7 mg of a sample of natural abundance $Zn(OAc)_2 \cdot 2H_2O$ with a contact time of 30 ms and a recycle delay of 5 s. A total of 100 spin echoes are accumulated. The inset is an expansion of the resulting Fourier transform of the time domain signal.

in Table 1 are the various NMR parameters of half-integer quadrupolar nuclides of potential biological interest. Included in the table are the relative Sternheimer antishielding factors $(1 - \gamma_\infty)$ (*22*), which we will use as a measure of the propensity of the given nuclide to have a quadrupole coupling different from zinc. The equations for the quadrupole coupling constant and the nuclear field gradient are given as

$$C_Q = q_{zz}^{\text{nuc}} \frac{e^2}{a_0^3 h} Q^{\text{X}} = q_{zz}^{\text{nuc}} Q^{\text{X}} 234.9649 \text{ MHz} \qquad [2]$$

$$q_{zz}^{\text{nuc}} = q_{zz}^{\text{ext}}(1 - \gamma_\infty). \qquad [3]$$

Here C_Q denotes the quadrupole coupling constant, and q_{zz}^{ext} and q_{zz}^{nuc} are the external and nuclear field gradients, respectively. Likewise, Q^{X} is the nuclear quadrupole moment in units of 10^{-24} cm^2, and the atomic constants a_0, e, and h have their usual meanings. Historically, field gradients were calculated using an external field gradient, and the result had to be modified via a Sternheimer antishielding factor $(1 - \gamma_\infty)$ (*22d*).

As illustrated above, the ^{67}Zn NMR experiment can be considered, if not routine, at least a "straightforward" experiment. Table 1, compares other half-integer quadrupole nuclides relative to the ease of performing the ^{67}Zn NMR experiment. If we assume, for the moment, that all of these nuclides have the same value for the quadrupole coupling constant, C_Q, then the relative ease of each experiment would follow the relative sensitivity for each nuclide. If this were the case, ^{25}Mg

TABLE 1
NMR Properties of Biologically Relevant Metals with Half-Integer Nuclear Spins

Atom	Spin	NMR frequency[a]	Sternheimer factors[b]	Relative quadrupole moment[c]	Relative sensitivity[d]
^{9}Be	$\frac{3}{2}$	56.212	~0 [0]	0.3467	4.24
^{23}Na	$\frac{3}{2}$	105.804	−6.0 [0.48]	0.8	162.22
^{25}Mg	$\frac{5}{2}$	24.48	−4.0 [0.32]	1.467	0.96
^{39}K	$\frac{3}{2}$	18.664	−19.5 [1.58]	0.367	0.27
^{43}Ca	$\frac{7}{2}$	26.912	−14.2 [1.15]	1.33[e]	2.07
^{51}V	$\frac{7}{2}$	105.16	−6.8 [0.55]	2	649.17
^{59}Co	$\frac{7}{2}$	94.456	−3.1 [0.25]	2.67	295.98
^{65}Cu	$\frac{3}{2}$	113.64	−20.5 [1.67]	−1	40.14
^{67}Zn	$\frac{5}{2}$	25.008	−12.3 [1]	1	1

[a] These frequencies correspond to a magnetic field of 9.4 T.

[b] The Sternheimer factors ($1 - \gamma_\infty$) are calculated using the methods outlined by Slichter (*22d*). See also the web page constructed by Harbison: http://wendigo.unl.edu/gerry/sternheimer.html. The values in [ ] are relative to the value for ^{67}Zn.

[c] The quadrupole moment of ^{67}Zn is 0.15×10^{-28} m^2. Values are from Table 1.2 of (*32*).

[d] The relative sensitivity was computed based on an equal number of nuclei and assuming the relative sensitivity is proportional to $\gamma^3 I(I+1)$.

[e] The quadrupole moment of ^{43}Ca is 0.2 ± 0.1. This corresponds to an uncertainty in the ratio of -0.667 to $+2$.

experiments would be comparable to that for ^{67}Zn, whereas the same experiment performed on ^{23}Na would be 162 times easier. However, the values of the quadrupole coupling constant are rarely the same in going from one nucleus to another. To make such a comparison, as a first approximation, the quadrupole moment of the nucleus in question can be used. In the examples cited above, the quadrupole moment for ^{25}Mg is about 50% larger than the moment for ^{67}Zn, whereas the quadrupole moment for ^{23}Na is slightly smaller than that for ^{67}Zn. However, the moment is not the whole picture, relative to the value of the quadrupole coupling constant, i.e., Eqs. [2] and [3]. Admittedly, when comparing one nucleus to another, the quadrupole moment argument is at best qualitative. For the purposes of this table, consider the relative Sternheimer factor as a measure of the propensity of the given nuclide to have a quadrupole coupling constant that is different from that of zinc. Comparing ^{25}Mg to ^{67}Zn, the information in Table 1 suggests that the two experiments should be comparable in difficulty. Namely, the NMR sensitivity for an equal number of nuclei is about the same, and the increased moment of ^{25}Mg is offset by a corresponding decrease in the Sternheimer factor. Likewise, by comparing ^{65}Cu to ^{67}Zn and considering only relative sensitivity and relative quadrupole moments, one would conclude *incorrectly* that the corresponding ^{65}Cu NMR experiments would be easy relative to ^{67}Zn. The relative Sternheimer factor suggests otherwise. The published quadrupole coupling constants for ^{65}Cu suggest coupling constants that are a factor of 3 to 5 times larger (*23*) than those observed for ^{67}Zn (typically $<$10 MHz). Analogously, the data in Table 1 would suggest the corresponding NMR experiments utilizing ^{39}K and ^{43}Ca would be more difficult than the corresponding ^{67}Zn experiment. However, if the quadrupole couplings constants are comparable, then the data in Table 1 argues that conditions can be found where ^{39}K (*6*) and ^{43}Ca (*24*) experiments can be performed as well. Admittedly, the ^{43}Ca experiment is more of a challenge at natural abundence. To illustrate these points we will compare the relative ease of performing ^{67}Zn and ^{25}Mg NMR experiments.

Due to the chemistry of magnesium and its importance in repair biology (*25*) ^{25}Mg was chosen as the next example. From the information in Table 1 one can see that for an equal number of spins, the corresponding ^{25}Mg NMR experiment is comparable in difficulty to that for ^{67}Zn. Further, at natural abundance (10.13% for ^{25}Mg) it should be more favorable by a factor of ~2.5. Presented in Fig. 6 are the ^{25}Mg CP/QCPMG results for a natural abundance sample of 143.9 mg of $Mg(OAc)_2 \cdot 4H_2O$. The tetrahydrate crystallizes in a

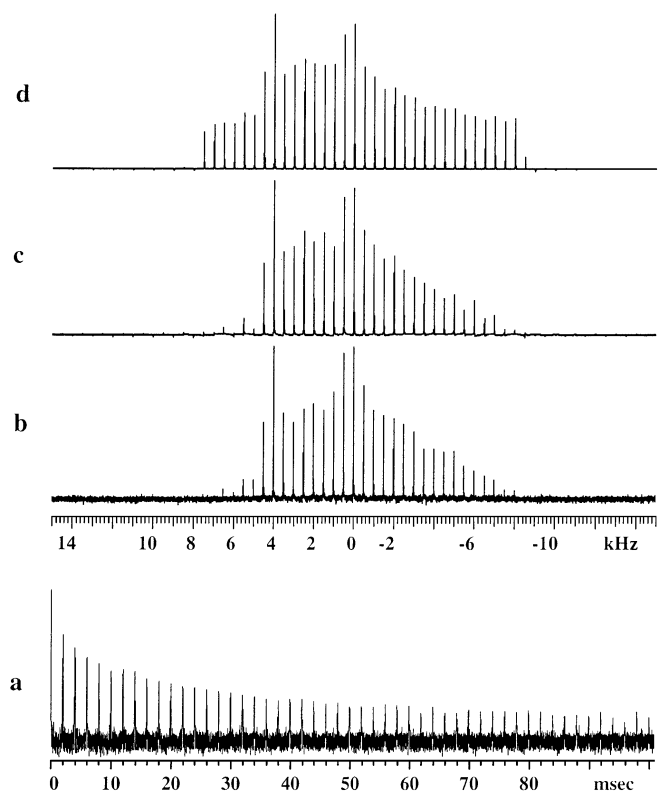

FIG. 6. (a) Time domain signal from 256 accumulations of a CP/QCPMG pulse sequence applied to 143.9 mg of a sample of natural abundance $Mg(OAc)_2 \cdot 4H_2O$ with a contact time of 30 ms. The total number of echoes is 50. The inset is an expansion of (b) the resulting Fourier transform of the time domain signal, (c) the simulated data using parameters described in the text using finite pulse widths, and (d) the same as in (c) except ideal pulses were used.

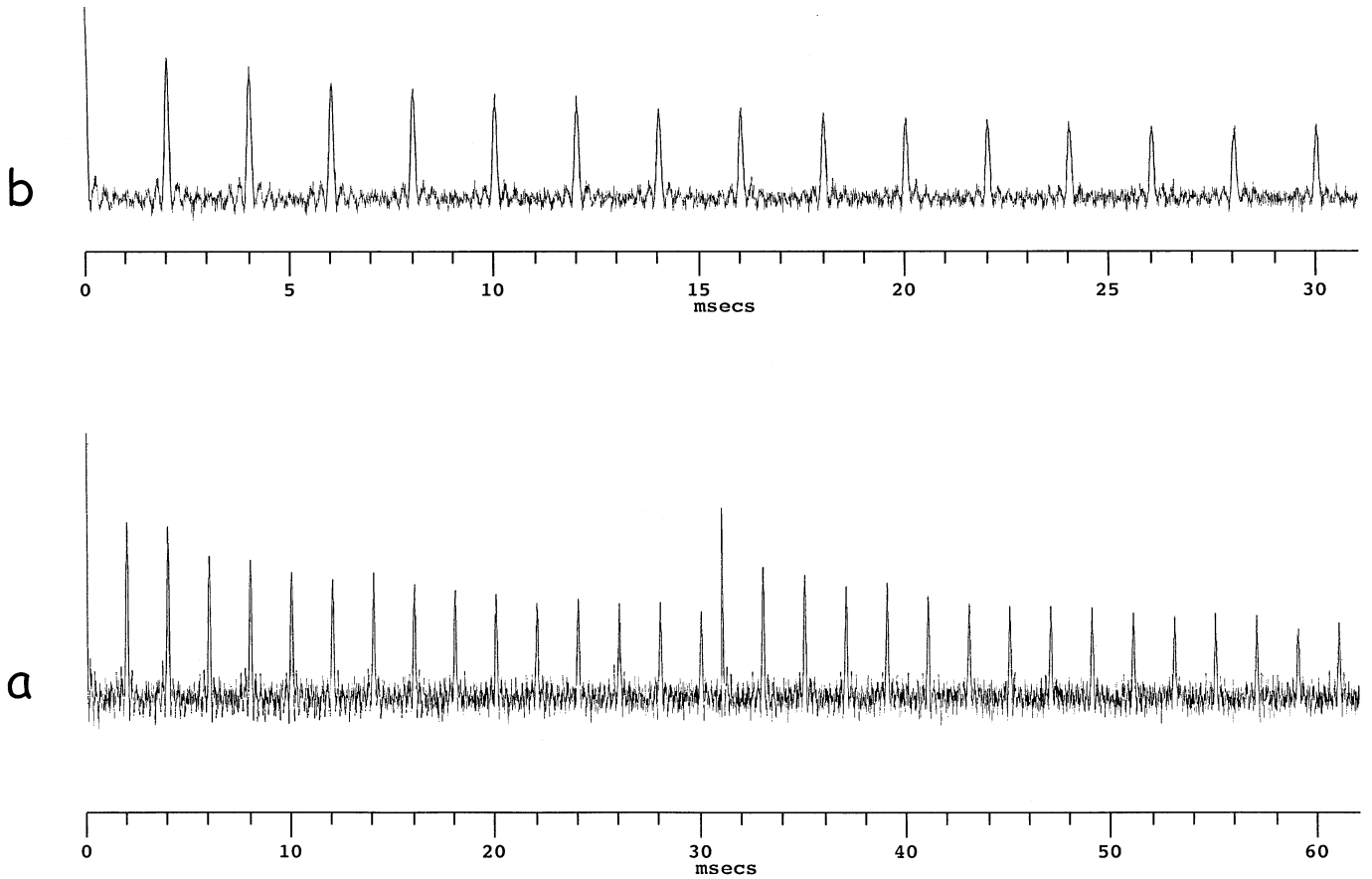

FIG. 7. (a) Time domain signal resulting from applying a multiple-contact (*2*) CP/QCPMG sequence to a sample of 143.9 mg of natural abundance $Mg(OAc)_2 \cdot 4H_2O$; successive acquisitions are concatenated with 64 accumulations at 50 K and a recycle delay of 20 s. (b) Time domain signal acquired with the same parameters as in (a) but with the signal coadded during the experiment.

monoclinic space group ($P2_1/c$) with $Z = 2$ (*26*). The two magnesium atoms are chemically and symmetry equivalent. Figure 6a denotes the time domain signal resulting from 50 spin echoes. Figure 6b denotes the simple Fourier transform of the signal in Fig. 6a. Figures 6c and 6d depict SIMPSON (*27*) simulations of finite and ideal pulses, respectively. The quadrupole coupling constant and asymmetry parameter extracted from the lineshape are 2.8 MHz and 0.67, respectively. The fit of the data did *not* improve by adding any shielding anisotropy. Like the spectrum of the zinc acetate, the magnesium acetate is of high S/N with only 256 accumulations (recycle time every 20 s). Hence, any conclusions relative to Zn^{2+}-metalloproteins can be carried over to the corresponding Mg^{2+}-depenedent proteins.

In both of the examples presented here the presence of methyl groups was used as a means to facilitate ^{1}H relaxation through tunneling (*28*). Due to the significant lengthening of the ^{1}H spin–lattice relaxation time T_1 we have not taken full advantage of the potential gains in S/N from dropping the temperature further. There are at least two ways of managing the ^{1}H T_1 values. The first approach involves the use of paramagnetic dopants; the results of those investigations will be the topic of a future publication. The second approach exploits common attributes of low-temperature NMR, i.e., typically long values for both the ^{1}H T_1's and $T_{1\rho}$'s. These attributes can be addressed by using multiple-contact experiments in combination with a ^{1}H flip-back pulse in the CP experiment. The utilization of these methods is illustrated with ^{25}Mg experiments in Figs. 7 and 8.

Figure 7 illustrates the importance of multiple-contact experiments. In high-resolution CP/QCPMG experiments, depending upon contact time and the number of echoes collected, the experiment may be limited to two contacts (due to the length of time the decoupler is on). In practice a limit of ~130 ms total of contact times and decoupling time was maintained. Figure 7a shows the signal resulting from each of the two contacts. The apparent losses due to ^{1}H $T_{1\rho}$'s between contacts is ~38%; however the gain in S/N over a single-contact version of the experiment is ~62%. With most of the proton magnetization apparently spin locked, it was worth attempting a flip back pulse after the last

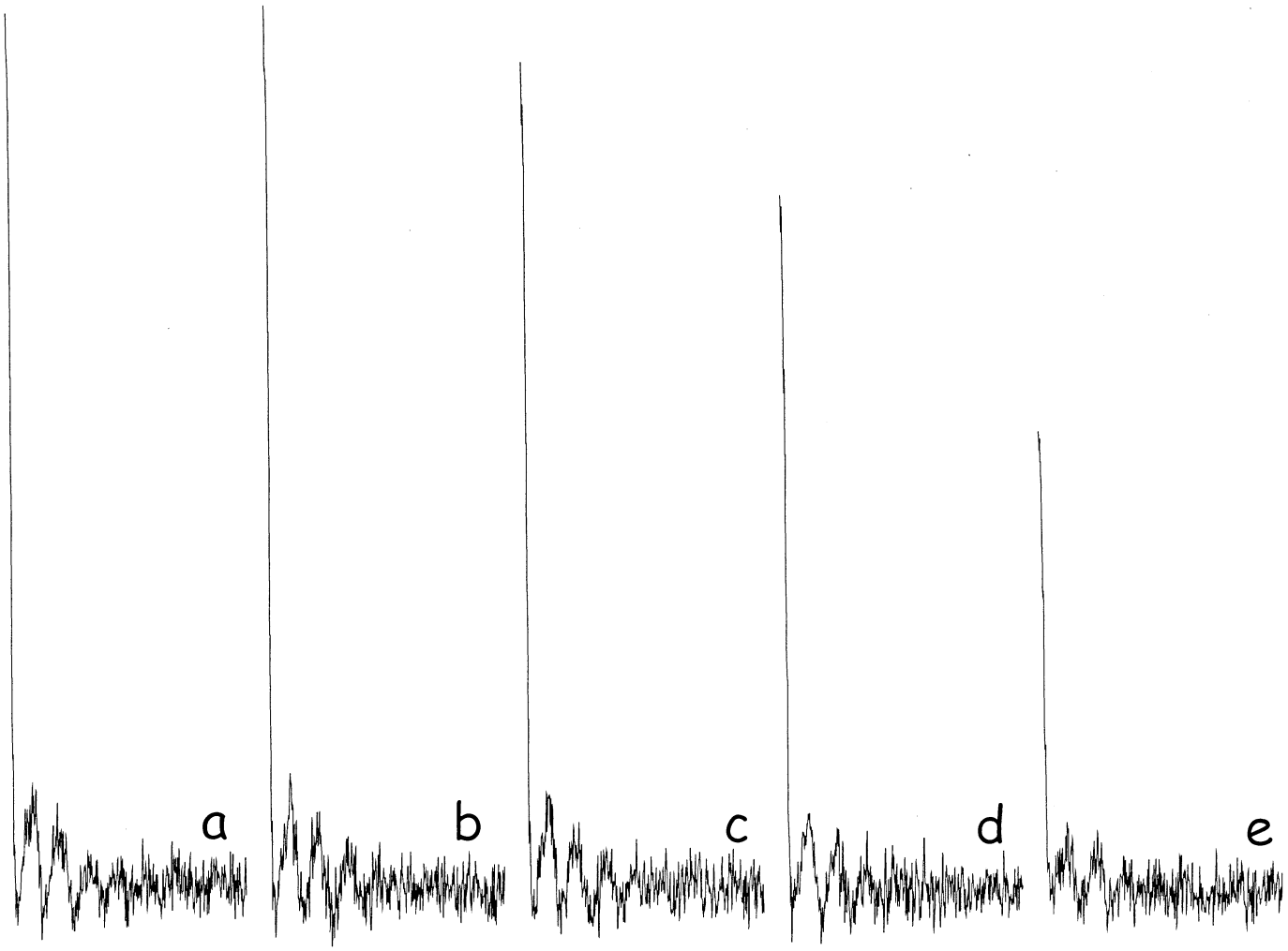

FIG. 8. The results of applying a multiple-contact (*2*) CP/QCPMG sequence utilizing a flip-back pulse to a sample of 143.9 mg of natural abundance $Mg(OAc)_2 \cdot 4H_2O$. The five time domain signals represent the result of 64 accumulations at 50 K. Each signal differs only in the recycle delay employed in the experiment. From (a) to (e), the values of the recycle delay are 20, 10, 5, 2.5, and 1 s respectively. The optimal recycle delay in the absence of the flip-back pulse is 20 s.

acquisition. These results are summarized in Fig. 8. The optimal recycle delay at this temperature for a normal single-contact CP/QCPMG for this sample is 20 s. As can be seen from the figure, there is essentially no loss in S/N (6%) when employing a ^{1}H flip-back pulse and a recycle delay 25% (5 s compared to 20 s) of the optimal. In the last case (1 s recycle time) the drop is only $\sim$50% of the data collected with an optimal delay.

DATA PROCESSING

Upon closer examination of the time domain signals (see Figs. 5–7), several data processing possibilities arise (*29*, *30*). The first obvious point is the presence of two decay times present within the induced signal. The first is the "slow" decay of the overall echo envelope. This decay determines the linewidth of the individual spikelets in the transformed spectrum. The second decay is associated with each half-echo and reflects the width of the static powder lineshape. For apodization of the second decay a Gaussian or a simple exponential function can be utilized with the proper symmetry between half-echoes and propagation for each echo of the train. This "matched" apodization function serves to reduce the noise, which is normally apodized in the standard processing of a single half-echo. Figures 9a–9c depicts the first 25 ms of a raw time domain signal, the "matched" apodization function (500 Hz exponential), and the product of the two.

A more subtle point arises in the use of zero filling. In the "normal" application, zero filling can be employed by adding the appropriate number of points at the *end* of the induced signal prior to Fourier transformation. However, the data can be

zero filled in another fashion. By adding an even number of zeroes between the echoes one can decrease the spacing of the spikelets in the frequency domain without adding noise. For example, consider the induced signal with an echo separation defined by 1000 points (500 points per half-echo) with a dwell time of 1 μs, or an echo separation of 1 ms. Fourier transformation of this signal results in a spikelet spectrum with a separation between the spikes of 1 kHz. Adding 1000 zeroes symmetrically between each of the half echoes, the echo separation becomes 2 ms (with a corresponding separation of 500 Hz between the spikes in the transformed data). In order to avoid artifacts that will arise because of the apparent signal truncation problems, the apodization procedure described above should be applied before Fourier transformation. The result should be a better representation of the actual lineshape. To illustrate this, consider again the time domain signal in Fig. 9a where the echo separation corresponds to 1 ms with a dwell time of 1 μs (1000 points between half-echoes). Figure 9d is apodized as in Fig. 9c; however we have doubled the length of each half-echo with zeroes. The comparison of the transformed data is depicted in Fig. 10, where the total number of points transformed was 512k.

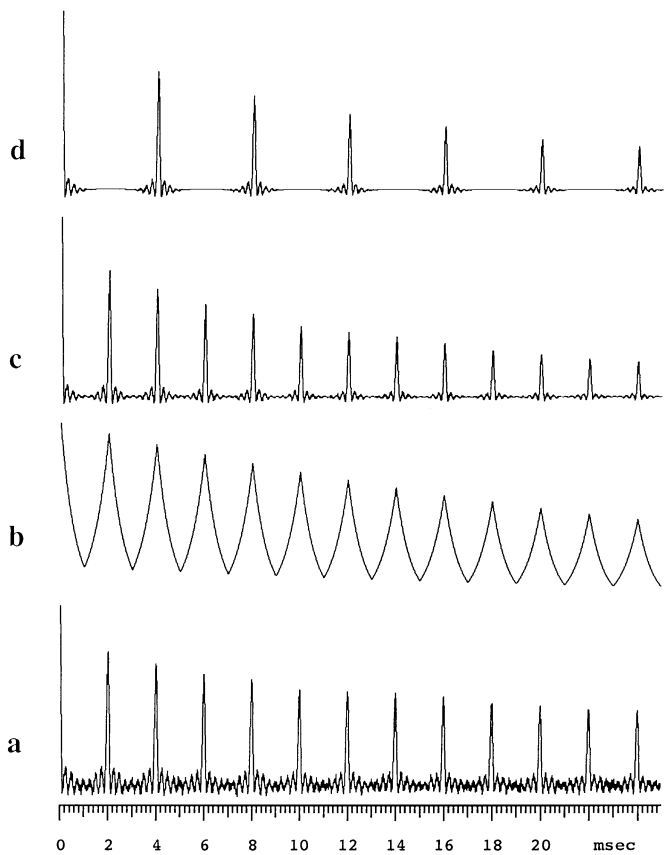

FIG. 9. The first 25 ms of time domain signal from the data pictured in Fig. 6. Depicted are (a) raw data, (b) the apodization function to be applied, (c) the resultant apodized signal, and (d) a zero-filled and apodized signal as described in the text.

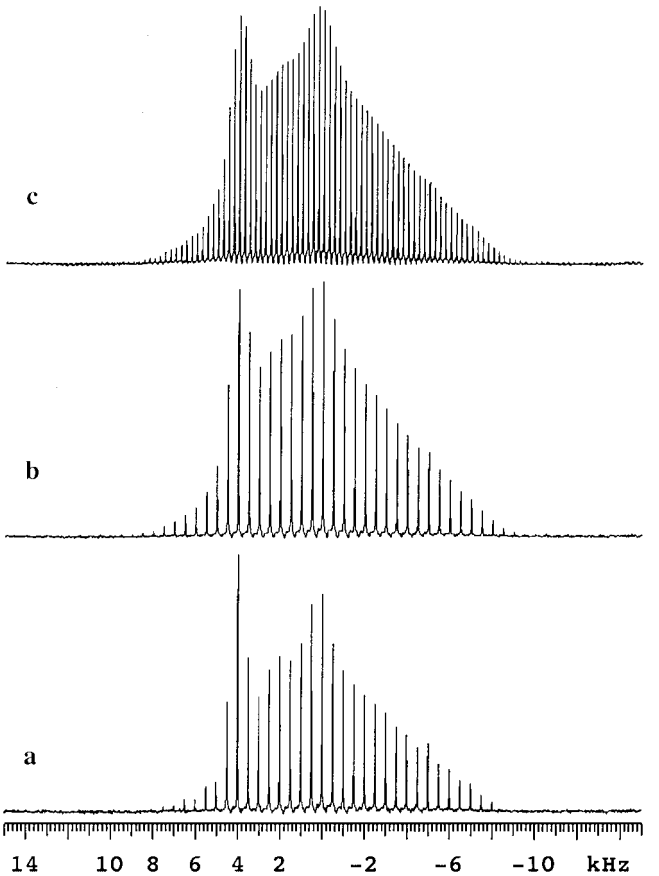

FIG. 10. Fourier-transformed data with conventional zero filling out to 512k points from Figs. 9a, 9c, and 9d, respectively.

CONCLUSIONS

The results presented here demonstrate that not only are ^{25}Mg and ^{67}Zn NMR experiments feasible, but there is sufficient sensitivity (with enrichment) that these nuclides can be examined in proteins. This level of optimism can also carry over to experiments using enriched ^{43}Ca (*24*). This represents the beginning of the utilization of the above-mentioned nuclides as a means to probe structure/function relationships by NMR spectroscopy. Even with today's 21 T magnets, if solution NMR methods afforded observable metal resonances in metalloproteins, the resulting linewidths (due to quadrupole relaxation) would be such as to obscure the determination of site-specific isotropic chemical shifts. In the absence of this shielding information, the utility of the approach is significantly weakened. Even in the case of a single site, the quadrupole coupling constant extracted from the data by itself, is not as easily correlated with structure in the absence of knowing the full quadrupole tensor (i.e., the asymmetry parameter, η). That level of detail can only be obtained by a solid state NQR or NMR experiment. This is further complicated in the presence of distinct, multiple sites. In the absence of independent information the resulting solution spectra are at best difficult to interpret.

Due to the difficulty in observing a broad, low-frequency resonance in solution NMR experiments 25 years ago, a surrogate probe strategy was developed (*31*). The strategy was the replacement of the metal of interest, in this case Ca^{2+} and Zn^{2+}, with Cd^{2+}. Allowing for the chemical differences between Cd^{2+} and Zn^{2+} and Ca^{2+}, the overall strategy was successful. The solid state ^{113}Cd experiments afforded a direct comparison of shielding tensors with X-ray structural data, thus providing the means to probe structure and function. With these data in hand, it became possible to utilize the chemical shift as a means to understand the consequences of the ligand environment on the shielding tensor in the protein of interest. The results presented here illustrate that this methodology (low-temperature NMR, cryogenic preamplifier, and CP/QCPMG) potentially provides the means to directly address correlations between quadrupole, shielding tensors, and their relative orientations with structure/functional information, obviating the need for the surrogate probe strategy.

The new methodology for direct observation of a half-integer quadrupolar nuclide discussed above is described as a general one. However, this is only true if the spin of interest is diluted in a matrix that is rich in protons (or some other spin that can provide a source of magnetization to the nuclide of interest). Although we have targeted biological systems, the method is certainly not limited to these environments. For example, probing Brønsted acidity on metal oxide surfaces would represent another potential application of this methodology, e.g., ZnO, MgO, and CaO just to mention three. In those systems where cross-polarization is not possible or practical, other approaches must be utilized (such as QCPMG alone with paramagnetic doping).

The importance of high magnetic fields in the solid state NMR experiment cannot be overstressed. The width of the second-order quadrupole lineshape, to first approximation, is inversely proportional to the Larmor frequency. In the near future, these same experiments will be implemented on a 18.8-T spectrometer. The increased field strength will undoubtedly afford higher sensitivity and, additionally, allow the measurement of the contribution of chemical shielding to the observed lineshapes. Therefore the combination of this technique and high magnetic field enables the determination of the desired correlation of magnetic resonance parameters with structure/function of the biological system.

ACKNOWLEDGMENTS

The authors thank Drs. Michael K. Bowman, Sarah D. Burton, David F. Lowry, and Robert A. Wind for helpful discussions. This work was supported in part by the National Institutes of Health (Federal Grant GM26295F) and by the Department of Energy Office of Biological and Environmental Research Program under Grant 24931 KP11-01-01. The research was performed in the Environmental Molecular Sciences Laboratory (a national scientific user facility sponsored by the DOE Biological and Environmental Research) located at Pacific Northwest National Laboratory and operated for DOE by Battelle.

REFERENCES

1. J. J. R. Frausto da Silva and R. J. P. Williams, "The Biological Chemistry of the Elements. The Inorganic Chemistry of Life," Clarendon Press, Oxford (1991).
2. L. I. Alberts, K. Nadassy, and S. J. Wodak, Analysis of zinc binding sites in protein crystal structures, *Protein Sci.* **7,** 1700–1716 (1998).
3. S. J. Lippard and J. M. Berg, "Principles of Bioinorganic Chemistry," University Science Books, Mill Valley, CA, (1994).
4. (a) G. E. Maciel, L. Simeral, and J. J. H. Ackerman, Effects of complexation on zinc(II) on zinc-67 chemical shifts, *J. Phys. Chem.* **81,** 262 (1977); (b) T. Shimizu and M. Hatano, Magnetic resonance studies of trifluoperazine-calmodulin solutions: ^{43}Ca, ^{25}Mg, ^{67}Zn, and ^{39}K nuclear magnetic resonance, *Inorg. Chem.* **24,** 2003 (1985).
5. (a) T. Vosegaard, U. Andersen, and H. J. Jakobsen, Improved ^{67}Zn solid state NMR from single crystal studies of $Zn(CH_3OO)_2 \cdot 2H_2O$, *J. Am. Chem. Soc.* **121,** 1970–1971 (1999); (b) G. Wu, Recent developments in solid-state nuclear magnetic resonance of quadrupolar nuclei and applications to biological systems, *Biochem. Cell Biol.* **76,** 429–442 (1998); (c) G. Wu, Zinc-67 nuclear magnetic resonance spectroscopy of solids, *Chem. Phys. Lett.* **298,** 375–380 (1998); (d) C. Debiemme-Chouvy, J. Vedel, M.-C. Bellissent-Funel, and M. R. Cortes, Supersaturated zincate solutions, *J. Electochem. Soc.* **142,** 1359–1364 (1995); (e) G. Wu, S. Kroeker, and R. E. Wasylishen, Multinuclear NMR study of dipotassium tetracyanometalates of the group 12 metals in the solid state, *Inorg. Chem.* **34,** 1595–1598 (1995); (f) Y. Ogoma, H. Shinshu, T. Fujii, Y. Kondo, A. Hachimori, T. Shimizu, and M. Hatano, Binding study of metal ions to S100 protein: Calcium-43, magnesium-25, zinc-67, and potassium-39, *Int. J. Biol. Macromol.* **14,** 279–286 (1992); (g) G. Gruette, B. Thomas, and D. Scheller, Zinc-67 and lithium-7 NMR of concentrated solutions of the ternary zinc chloride–lithium chloride–water systems, *Z. Chem.* **30,** 181 (1990); (h) F. H. Larsen, A. S. Lipton, H. J. Jakobsen, N. C. Nielsen, and P. D. Ellis, ^{67}Zn QCPMG solid-state NMR studies of zinc complexes as models for metalloproteins, *J. Am. Chem. Soc.* **121,** 3783 (1999); (i) F. H. Larsen, J. Skibsted, H. J. Jakobsen, and N. C. Nielsen, Solid-state QCPMG NMR on low γ quadrupolar metal nuclei in natural abundance, *J. Am. Chem. Soc.* **122,** 7080–7086 (2000).
6. A. C. Kunwar, G. L. Turner, and E. Oldfield, Solid-state spin-echo Fourier transfrom NMR of ^{39}K and ^{67}Zn salts at high field, *J. Magn. Reson.* **69,** 124 (1986).
7. (a) A. Llor and J. Virlet, Towards high resolution NMR of more nuclei in solids; sample spinning with time dependent spinner axis angle, *Chem. Phys. Lett.* **152,** 248 (1988); (b) K. T. Mueller, B. Q. Sun, G. C. Chingas, J. W. Zwanziger, T. Terao, and A. Pines, Dynamic angle spinning of quadrupolar nuclei, *J. Magn. Reson.* **86,** 470 (1990).
8. A. Samoson, E. Lippmaa, and A. Pines, High resolution solid-state NMR. Averaging of second order effects by means of a double-rotor, *Mol. Phys.* **65,** 1013 (1988).
9. L. Frydman and J. S. Harwood, Isotropic spectra of half-integer quadrupolar spins from bidimensional magic angle spinning NMR, *J. Am. Chem. Soc.* **117,** 5367 (1995).
10. D. I. Hoult and R. E. Richards, *Electron. Lett.* **11,** 596 (1975).
11. P. Styles, N. F. Soffe, C. A. Scott, D. A. Cragg, R. Row, D. J. White, and P. C. White, A high resolution NMR probe in which the coil and preamplifier are cooled with liquid helium, *J. Magn. Reson.* **60,** 397 (1984); P. Styles and N. F. Soffe, An improved cryogenically cooled probe for high-resolution NMR, *J. Magn. Reson.* **84,** 376 (1989).
12. A. Pines, M. G. Gibby, and J. S. Waugh, Proton enhanced nuclear induction spectroscopy. A method for high resolution NMR of dilute spins in the solids, *J. Chem. Phys.* **56,** 1776 (1972).
13. M. M. Maricq and J. S. Waugh, *J. Chem. Phys.* **70,** 3300 (1979).

14. (a) H. Y. Carr and E. M. Purcell, Effects of diffusion on free precession in nuclear magnetic resonance experiments, *Phys. Rev.* **94,** 630 (1954); (b) S. Meiboom and D. Gill, Modified spin-echo method for measurement of nuclear relaxation times, *Rev. Sci. Instrum.* **29,** 688 (1958).

15. A. N. Garroway, Homogeneous and inhomogeneous nuclear spin echoes in organic solids: Adamantane, *J. Magn. Reson.* **28,** 365 (1977).

16. F. H. Larsen, H. J. Jakobsen, P. D. Ellis, and N. C. Nielsen, Sensitivity-enhanced quadrupolar-echo NMR of half-integer quadrupolar nuclei. Magnitudes and relative orientation of chemical shielding and quadrupole coupling tensors, *J. Phys. Chem.* **101,** 8597 (1997).

17. Y. W. Kim, W. L. Earl, and R. E. Norberg, Cryogenic probe with low-loss transmission line for nuclear magnetic resonance, *J. Magn. Reson. A* **116,** 139–144 (1995).

18. R. A. McKay, Probes for special purposes, *in* "Encyclopedia of Nuclear Magnetic Resonance" (D. M. Grant and R. K. Harris, Eds.), Vol. 6, pp. 3768–3771, Wiley, New York (1996).

19. S. R. Hartmann and E. L. Hahn, Nuclear double-resonance in the rotating frame, *Phys. Rev.* **128,** 2042 (1962).

20. (a) S. Vega, *Phys. Rev.* **23,** 3152 (1981); (b) T. H. Walter, G. L. Turner, and E. Oldfield, Oxygen-17 cross-polarization NMR spectroscopy of inorganic solids, *J. Magn. Reson.* **76,** 106 (1988).

21. A. S. Lipton, J. A. Sears, and P. D. Ellis, Solid state NMR of biologically relevant metals, poster at the 41st Experimental NMR Conference at Pacific Grove, CA, April 9–14, 2000, unpublished results.

22. (a) R. M. Sternheimer, *Phys. Rev.* **84,** 244 (1951); (b) R. M. Sternheimer, *Phys. Rev.* **86,** 316 (1952); (c) R. M. Sternheimer, *Phys. Rev.* **95,** 736 (1954); (d) C. P. Slichter, "Principles of Magnetic Resonance," third ed., Chap. 10, Springer-Verlag, New York (1990).

23. M. -Y. Liao, R. Subramanian, and G. S. Harbison, Two and three dimensional nuclear quadrupole resonance in the investigation of structure and bonding, *Z. Naturforsch. A* **55,** 29–36 (2000).

24. R. G. Bryant, S. Ganapathy, and S. D. Kennedy, High-resolution calcium-43 NMR in solids, *J. Magn. Reson.* **72,** 376–378 (1987).

25. R. B. Martin, Bioinorganic chemistry of magnesium, *in* "Compendium on Magnesium and its Role in Biology, Nutrition, and Physiology. Metal Ions in Biological Systems" (H. Segael, Ed.), Vol. 26, pp. 1–14, Marcel Decker, New York (1990).

26. D. E. Irish, J. Semmler, N. J. Taylor, and G. E. Toogood, Structure of magnesium diacetate tetrahydrate, *Acta Crystallogr. Sect. C* **47,** 2322–2324 (1991).

27. M. Bak, J. T. Rassmussen, and N. C. Nielsen, SIMPSON: A General Simulation for Solid State NMR Spectroscopy, *J. Magn. Reson.* **147,** 296–330 (2000).

28. R. A. Wind, S. Emid, D. J. Ligthelm, J. F. J. M. Pourquié, and J. Smidt, The impact of the symmetry properties of classical reorienting and tunneling methyl groups on the spin-lattice relaxation in solids, *Bull. Magn. Reson.* **6,** 71–88 (1984).

29. R. R. Ernst, G. Bodenhausen, and A. Wokaum, "Principles of Nuclear Magnetic Resonance in One and Two Dimensions," Chap. 4, pp. 99–111, Oxford Science, Clarendon Press, Oxford (1991).

30. J. C. Hoch and A. S. Stern, "NMR Data Processing," Chap. 3, Wiley, New York (1996).

31. A. D. Cardin, P. D. Ellis, J. D. Odom, and J. W. Howard, Jr., Cadium-113 Fourier transform nuclear magnetic resonance spectroscopy, *J. Am. Chem. Soc.* **97,** 1672–1680 (1975); I. M. Armitage, R. T. Pajer, A. J. M. S. Uiterkamp, J. F. Chlebowski, and J. E. Coleman, Cadmium-113 Fourier transform nuclear magnetic resonance spectroscopy of cadmium(II) carbonic anhydrases and cadmium(II) alkaline phosphatase, *J. Am. Chem. Soc.* **98,** 5710–5712 (1976); P. D. Ellis, Cadmium-113 magnetic resonance spectroscopy, *Science* **221,** 1141–1146 (1983); M. F. Summers, Cadmium-113 NMR spectroscopy of coordination compounds and proteins, *Coord. Chem. Rev.* **86,** 43 (1988); J. E. Coleman, *in* "Metallobiochemistry" (J. F. Riordan and B. L. Vallee, Eds.), *Methods in Enzymology*, Vol. 227, Part D, pp. 16–43, Academic Press, San Diego (1993).

32. R. K. Harris, *in* "NMR and the Periodic Table" (R. K. Harris and B. E. Mann, Eds.), pp. 6–7, Academic Press, London (1978).